

Quantitative Susceptibility Mapping: High Resolution Imaging of the Dentate Nucleus at High Field Strength (7T)

PINAR SENAY ÖZBAY^{1,2}, Michael Wyss², Cristina Rossi¹, Klaas Paul Prüssmann², and Daniel Nanz¹

¹University Hospital Zürich, Institute for Diagnostic and Interventional Radiology, Zürich, Zürich, Switzerland, ²Institute for Biomedical Engineering, University and ETH Zürich, Zürich, Zürich, Switzerland

Target Audience: Researchers who are interested in susceptibility, QSM, T2* imaging and Dentate Nucleus.

Purpose: The aim of this study was to (i) visualize the fine convoluted band of the dentate nucleus (DN) (Fig.1) and to (ii) quantitatively measure its magnetic susceptibility in relation to that of white matter by means of high-resolution quantitative susceptibility mapping (QSM) in healthy volunteers at 7 Tesla. So far attempts at visualization of the gyrating band of the dentate nucleus have proven difficult, even with high-resolved MRI at 7 Tesla¹, which prevents a meaningful characterization, e.g., iron-content estimation, or differentiation of motor and non-motor subregions². We tested whether QSM would allow an improved visualization of the dentate nucleus as a prerequisite for a better understanding of pathologies related to cerebellar dysfunction³.



Fig1.) Anatomical view of dentate nucleus¹⁴

Materials and Methods: Three-dimensional T2*-weighted multi-gradient-echo images of 4 consenting volunteers (2 right-handed (RH), 2 left-handed (LH)) were acquired (TI FFE, FA = 18, TR = 60, TE = 5, 10, 15, 20, 25, 30, 35, 40, 45, 50 ms, voxel dimensions = 0.4, 0.4, 0.65 mm, and matrix size = 512x512x90), on a 7T MRI system (Achieva, Philips Healthcare, Cleveland, USA). Dicom magnitude T2* and real and imaginary images were obtained from the scanner and used for post-processing. Weighted phase increments, WPI , per echo-time increment were calculated, assuming a linear phase evolution⁴, $WPI = \text{angle}(\frac{1}{N} \sum_{n=1}^N S_n^* S_{n+1})$, N = number of echo times, S = complex signals, then unwrapped and subject to background-field removal by the Laplacian-based SHARP (threshold parameter = 0.1) method^{5,6}. Background noise and convolution artifacts were reduced by element-wise multiplication with the eroded binary whole-brain mask. Quantitative susceptibility, ΔX , maps were obtained from the SHARP images (WPI_s) by an inversion, using the relation $\Delta X = FT^{-1}(\frac{FT(-WPI_s)}{g}) / (\gamma B_0 \Delta TE)$, $g = \frac{1}{3} - \frac{k_z^2}{k^2}$, $k^2 = k_x^2 + k_y^2 + k_z^2$, where FT = Fourier Transform, γ = gyromagnetic ratio, B_0 = field strength, ΔTE = echo-time increment. Threshold based k-space division was applied with a threshold of 0.25, and the inverse was scaled by multiplying with the square of “ $g / 0.25$ ” to smooth thresholding-induced discontinuities^{4,5,7}. Regions of interest (ROI) in the dentate nucleus and white matter were drawn on the QSM in the image-processing program ImageJ⁸. Susceptibility differences with respect to white matter and volumes for the right and left dentate nucleus are reported.

Results & Discussion: Figure 2 shows exemplary T2* (a, c) and susceptibility maps (b, d) at identical location from volunteer LH-1. The detailed structure of cerebellum, and dentate nucleus, especially the corrugated walls and hilus, were generally better visible on the susceptibility maps than on the T2* images.

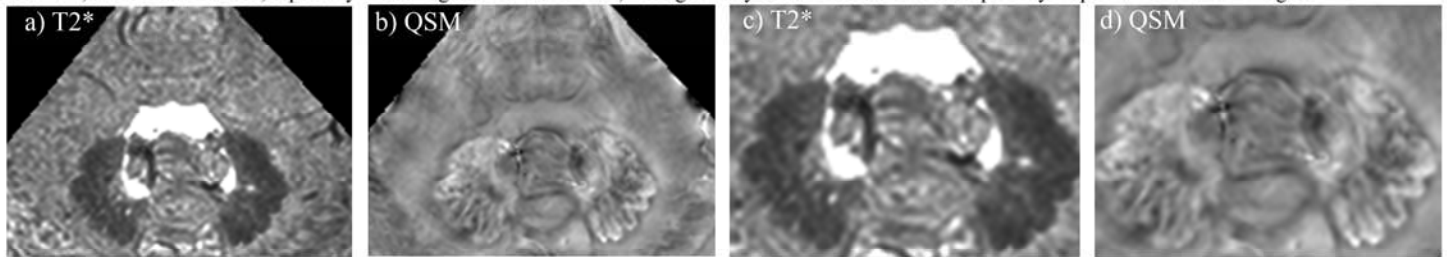


Fig2. T2* (a,c) and QSM (b,d) at identical location, volunteer LH-1, 0.4mm in plane resolution at 7T

Fig3. QSM of left dentate nucleus of volunteer LH-1, thin and thick lines outlining micro- and macrogyric regions, respectively (values in ppb)

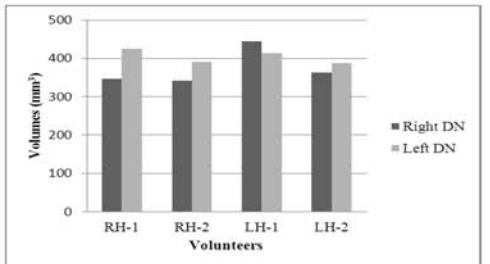
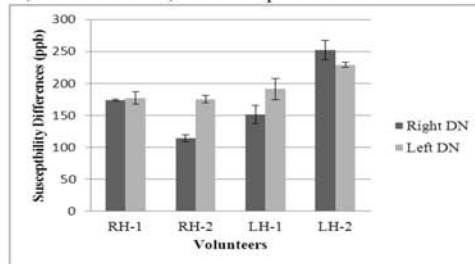
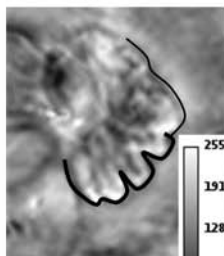


Fig 4: Susceptibility differences (left) and volumes (right) of right and left dentate nucleus of 4 volunteers.

Figure 4 summarizes the susceptibility differences with respect to white matter (left) and volume estimates (right) for right and left DN, mean values within each ROI were given with standard deviations. Average susceptibility differences vs. white matter across the volunteers were calculated as 162 ± 29 ppb and 184 ± 12 ppb for the DN in the right and left hemisphere, respectively. Our values represent averages in the narrow band of the DN only, and are significantly larger than susceptibility differences averaged over the whole bean-shaped outline of the nuclei that were reported in earlier works^{9,10}. Some of our maps suggest that susceptibility differences may even allow a differentiation of microgyric and macrogyric parts of the dentate nucleus, which are known to differ in iron content^{11,12}. E.g., **Figure 3** implies wider and more subdivided macrogyric parts of the posterior dentate nucleus than in the microgyric frontal parts. Although the segmentation of the DN band was straightforward on some slices, the contrast, even on the susceptibility maps, was too low in other slices to allow an accurate measurement of the whole volume of dentate nucleus. Our best-attempt estimates of mean DN volume across volunteers were $355 \text{mm}^3 \pm 24$ and $402 \text{mm}^3 \pm 9$ for right and left-DN, respectively, i.e. roughly 2 times larger than estimates from histology (155mm^3 ¹³). While the over-estimation with regard to histology may primarily be caused by erroneous segmentation and MRI partial volume artifacts, there might also be systematic differences associated with ex-vivo shrinkage¹⁰. In both RH volunteers, Left DN >> Right DN, while for volunteer LH-2 Left DN > Right DN and for volunteer LH-1, Left DN < Right DN. Standard deviations for susceptibility differences and volume estimates across volunteers were larger for Right-DN than for Left-DN.

Conclusion: We report, for the first time to the best of our knowledge, quantitative susceptibility differences between the gyrating dentate-nucleus band and white matter, which was, in part, imaged with excellent contrast. However, the depiction of the DN band was not consistently sufficient for the volume estimations to match results based on histology. In contrast to traditional MR imaging techniques QSM may be able to map dentate nucleus in sufficient detail to offer new possibilities regarding (i) visualization and segmentation of DN and (ii) characterization, e.g., of the iron content.

References: [1] Maderwald et al., NeuroImage 63 (2012) 1421–1431 [2] Kuper et al., NeuroImage 54 (2011) 2612–2622 [3] Frismand et al., NeuroImage: Clinical 2 (2013) 542–548 [4] Ozbay et al., Int. Workshop on MRI Phase Contrast & QSM, p18, 2013 [5] Schweser et al., Magnetic Resonance in Medicine 69:1582–1594 2013 [6] Schofield and Zhu, Opt. Lett. 28(14):1194–6 2003 [7] Haacke et al., J Magn Reson Imaging 32(3):663–76 2010 [8] Abramoff et al., Biophotonics International, 11(7) :36–42, 2004 [9] Lim et al., Neuroimage, 82:449–69 2013 [10] Bilgic et al., Neuroimage 59, 2625–2635 2012 [11] Diedrichsen, Neuroimage 54:1786–1794 2011 [12] Deoni and Catani, Neuroimage, 37(4):1260–6 2007 [13] Höpker et al., Z. Altersforschung 5, 256–277 [14] http://en.wikipedia.org/wiki/Deep_cerebellar_nuclei